







Martian Atmospheric Spectral End-Members Retrieval From ExoMars Thermal Infrared (TIRVIM) Data

G. Alemanno¹ , M. D'Amore¹ , A. Maturilli¹, J. Helbert¹ , G. Arnold^{1,2}, O. Korabiev³ ,
N. Ignatiev³, A. Grigoriev⁴, A. Shakun³ , and A. Trokhimovskiy³ 

¹Institute for Planetary Research, German Aerospace Center DLR, Berlin, Germany, ²University of Potsdam, Institute of Geosciences, Potsdam, Germany, ³Space Research Institute (IKI), Moscow, Russia, ⁴Australian National University, Canberra, ACT, Australia

Special Section:

ExoMars Trace Gas Orbiter -
One Martian Year of Science

Key Points:

- First successful application of principal components and target transformation techniques to high-resolution Thermal Infrared channel (TIRVIM) data
- Spectral shapes of both atmospheric dust and water ice clouds are recognized and recovered
- TIRVIM data are successfully modeled through a linear combination of the recovered water ice and dust end-members

Supporting Information:

Supporting Information may be found in the online version of this article.

Correspondence to:

G. Alemanno,
Giulia.Alemanno@dlr.de

Citation:

Alemanno, G., D'Amore, M., Maturilli, A., Helbert, J., Arnold, G., Korabiev, O., et al. (2022). Martian atmospheric spectral end-members retrieval from ExoMars Thermal Infrared (TIRVIM) data. *Journal of Geophysical Research: Planets*, 127, e2022JE007429. <https://doi.org/10.1029/2022JE007429>

Received 24 JUN 2022

Accepted 25 AUG 2022

Abstract Key knowledge about planetary composition can be recovered from the study of thermal infrared spectral range datasets. This range has a huge diagnostic potential because it contains diagnostic absorptions from a planetary surface and atmosphere. The main goal of this study is to process and interpret the dataset from the Thermal Infrared channel (TIRVIM) which is part of the Atmospheric Chemistry Suite of the ExoMars2016 Trace Gas Orbiter mission to find and characterize dust and water ice clouds in the atmosphere. The method employed here is based on the application of principal component analysis and target transformation techniques to extract the independent variable components present in the analyzed dataset. Spectral shapes of both atmospheric dust and water ice aerosols have been recovered from the analysis of TIRVIM data. The comparison between our results with those previously obtained on Thermal Emission Spectrometer (TES) data and with previous analysis on TIRVIM data, validates the methodology here applied, showing that it allows to correctly recover the atmospheric spectral endmembers present in the TIRVIM data. Moreover, comparison with atmospheric retrievals on PFS, TES and IRIS data, allowed us to assess the temporal stability and homogeneity of dust and water ice components in the Martian atmosphere over a time period of almost 50 years.

Plain Language Summary The analysis of thermal infrared datasets from planetary bodies is of key importance for the understanding of a planet's climate evolution and history: it contains valuable information about composition, temperature and state of the atmosphere. Moreover, surface properties and the surface-atmosphere interaction can be studied. Here we investigated new thermal infrared data from the Thermal Infrared channel instrument of the ExoMars Trace Gas Orbiter with the main goal of carefully identifying Martian atmospheric dust and water ice clouds components. A methodology based on principal component and target transformation factor analysis techniques has been applied. Based on our results, this methodology can correctly recover both atmospheric dust and water ice aerosols spectral shapes and their abundances in the Martian atmosphere.

1. Introduction

Gases in the Martian atmosphere, aerosols, and the surface materials show absorption features in the thermal infrared range (~5–50 μm) (Christensen, 1998; Christensen et al., 1998; Conrath et al., 1973; Hanel et al., 1972; Martin & Richardson, 1993; Smith, Bandfield, & Christensen, 2000). The thermal emission signal includes both the emitted radiance determined by the surface temperature and the radiance components caused by spectrally selective absorptions of atmospheric and surface constituents (Bandfield & Smith, 2003). The disentanglement of these different radiation components is challenging but also implies a huge potential for the analysis of the thermal infrared spectral region—it provides a large and broad amount of information on the planet surface (such as composition, temperature and its state) as well as on its atmosphere and interaction between each other. A good atmospheric components retrieval is a first and a key step for a careful interpretation of the surface contribution.

Several spectral data have been collected so far from the Martian surface. The information supplied by OMEGA (Observatoire pour la Minéralogie, l'Eau, les Glaces et l'Activité, Bibring et al., 2006; Poulet et al., 2005) and CRISM (The Compact Reconnaissance Imaging Spectrometer for Mars; Murchie et al., 2007) in the Near-InfraRed (NIR) has been extended by TES (Thermal Emission Spectrometer; Christensen et al., 1992) and PFS (Planetary Fourier Spectrometer; Formisano et al., 2005) in the Thermal-InfraRed (TIR). The TES instrument is a Fourier

© 2022. The Authors.

This is an open access article under the terms of the [Creative Commons Attribution License](https://creativecommons.org/licenses/by/4.0/), which permits use, distribution and reproduction in any medium, provided the original work is properly cited.

Transform Michelson Interferometer covering the wavelength range from 6–50 μm with a spectral resolution of 5 and 10 cm^{-1} (Christensen et al., 1992) and bore-sighted visible/near-infrared (0.3–3.5 μm) and thermal (5–100 μm) bolometers. PFS onboard the ESA Mars Express (MEX) spacecraft is a double pendulum Fourier Transform interferometer covering the wavelength range from 1.2 to 5.5 μm (Short Wavelength channel—SW) and from 5.5 to 45 μm (Long Wavelength channel—LW). Spectral resolution of both channels is 1.3 cm^{-1} with a FOV of about 1.6 deg and of 2.8 deg for the SW and LW channel, respectively (Formisano et al., 2005). The analysis of TES data allowed carbonates detections in the Martian dust (Bandfield & Smith, 2003). The Mars Exploration Rovers Spirit and Opportunity also carried out a miniaturized version of TES (Christensen et al., 2003) to explore the surroundings of the landing areas.

Among the many approaches to separate atmospheric and surface signatures, two are particularly promising and will be pursued in the following approach. One algorithm is based on a combination of radiative transfer and subsequent least squares fitting. The second algorithm consists, instead, of a combination of principal component analysis, target transformation, and deconvolution techniques (Bandfield et al., 2000). Both methodologies have their advantages and disadvantages and three main differences can be pointed out:

- in the data used - while radiative transfer uses opacity spectra, deconvolution technique uses equivalent emissivity spectra. The use of opacity spectra is good when working with atmospheric components but not ideal for describing surface emissivity. On the other hand, the use of emissivity spectra, reasonable for describing the surface, cannot retrieve accurate quantitative abundances for each atmospheric absorption (Smith et al., 2000).
- in the spectral shapes computation - the radiative transfer algorithm is based on a sequential procedure that at first finds the spectral shape of the dust, then the one of the water-ice and it extracts in the end the surface emissivity. Combining principal component analysis and deconvolution algorithms it is, instead, possible to derive all the three shapes at the same time (Bandfield et al., 2000; Smith et al., 2000). On the other hand, if the single components vary synchronously, decoupling dust and water-ice contribution and single spectral shapes is more difficult.
- in the determination of the surface emissivity spectral shapes - radiative transfer algorithm performs an unconstrained fitting that has then to be correlated using mixing coefficients for dust and water-ice. This procedure requires an additional separate step that can add uncertainties. Adopting a deconvolution methodology one can avoid this extra step by using a spectral library of mineral spectral shape to perform a constrained fitting and derive the surface spectral shape. On the other hand, it is important also to know that this algorithm cannot produce spectra that are not in the spectral library, while the radiative transfer can.

Based on this, it is clear that it is not possible to assess the superiority of a model with respect to the other one but comparison between results obtained from both models could give a better interpretation of Martian orbital spectral data. In this paper, we show the first application of a method based on PCA and target transformation analysis techniques to spectral data from the Thermal Infrared Channel (TIRVIM) of the Atmospheric Chemistry Suite (ACS) of the ExoMars2016 Trace Gas Orbiter (TGO) (Korablev et al., 2018) and we compare the results obtained with this technique with those retrieved from the application of a radiative transfer model (Guerlet et al., 2022). Our investigation moves on two parallel tracks: the analysis of the new TIRVIM data set and the improvement of the Berlin emissivity spectral library (Alemanno et al., 2021) for the forthcoming interpretation of spectral surface endmembers. The TIRVIM channel, as TES and PFS, covers the spectral range where diagnostic features of water-alteration minerals are present. In particular, in the case of carbonates: lattice vibration bands and vibration fundamental bands occur at the wavelengths of ~ 7 , ~ 11.5 and ~ 14 μm (Adler & Kerr, 1962; Huang & Kerr, 1960). Strong overtone and combination bands are visible around ~ 3.4 – 3.5 and ~ 3.9 μm . High order overtones occur in the shortwave infrared around ~ 2.3 and ~ 2.5 μm , but those bands are intrinsically weaker (Wray et al., 2016). Therefore, the spectral range covered by TIRVIM has the potential to provide valuable information on the surface composition. However, in this range the spectral contrast and the spectral shape of compositional absorption features are affected by a number of physical effects due to particle-size distribution and single-scattering albedo (Bandfield, 2002). To correctly analyze the diagnostic feature for the surface composition, a correct retrieval of the atmospheric components is necessary. Moreover, the information on dust and water ice clouds is useful for characterization of dust and water atmospheric cycles and the understanding of the Martian climate: suspended particles of dust and water ices strongly influence the heat transportation and the thermal balance in the planet's atmosphere, as observed in the last Global Dust Storm (GDS) in the 2018/Martian year (Luginin et al., 2020).

In this paper we focus on showing the results of the retrieval of particulate atmospheric contributions to the selected TIRVIM spectral data. Analyzed data cover both regions of low and high emissivity. In regions of high emissivity, the surface contribution has been proved to be negligible (Bandfield et al., 2000). However, at other locations surface components are proved to be consistently present (Maturilli et al., 2009); the work presented here is the first result of a bigger work that shows how those techniques work and allow the retrieval of the atmospheric components when applied to TIRVIM data. The aim of this manuscript is to show this and some examples of the results obtained.

The adopted methodology has its roots in Bandfield et al. (2000) approach and uses Target Transformation (TT) and PCA techniques to analyze a set of mixed spectra and extract from that the number of independently variable components to recover the spectral end-members present in the data. It has been proved that three main atmospheric endmembers can be identified and combined linearly to model Martian TIR spectra: atmospheric dust, water ice clouds and a blackbody (Bandfield et al., 2000). In addition, as far as the modeling of the surface contribution is concerned, several works (i.e., Feely & Christensen, 1999; Gillespie, 1992; Hamilton & Christensen, 2000; Ramsey & Christensen, 1998; Ramsey & Fink, 1999; Ramsey et al., 1999; Thomson and Salisbury, 1993) showed that it is possible to approximately model the TIR spectra of a mixed surface through a linear combination of the end-members spectra, where each end-member is weighted by its areal concentration. To separate and extract each individual mineral contribution to the surface emissivity spectra, several deconvolution techniques have been tested (Bandfield, 2002; Feely & Christensen, 1999; Hamilton & Christensen, 2000; Hamilton et al., 1997; Ramsey & Christensen, 1998; Wyatt et al., 2001). These linear deconvolution models can be extended to the surface-atmosphere interaction in the Martian TIR spectra. Smith et al. (2000a, 2000b) showed that infrared observations on warm surfaces (>245 K) could be described through a linear model that combines a limited set of proper surface and atmospheric end-members.

D'Amore et al. (2013) applied multivariate techniques to PFS data confirming that these data can be fully described using a linear model that combines a set of end-member spectra identified by means of a TT technique (D'Amore et al., 2013). The method was applied on a set of PFS measurements in the same region where OMEGA detected the phyllosilicates on Mars. Once all the atmospheric endmembers are identified and characterized, for each PFS measured spectrum the residual of this fitting algorithm identifies the surface spectral residuum (Maturilli et al., 2009). This curve was again fitted by using a linear deconvolution of emissivity laboratory spectra for Martian analogue minerals, contained in the Berlin Emissivity Database (BED, Maturilli et al., 2008). This study shows that extracting information about the Martian surface using PFS observations is possible and it has the potential of providing useful hints on its composition (Maturilli et al., 2009). These first results show that one can successfully retrieve surface information from the Thermal infrared orbital datasets of the Red Planet.

Taking advantage of these results, this work aims at adopting this methodology to TIRVIM data, thus showing the potential of this method to retrieve first the different contributions from this dataset and in the future the potential of the dataset to contain valuable information about the Martian surface composition.

2. Instrument and Data Set

The ExoMars2016 Trace Gas Orbiter (TGO) has an Atmospheric Chemistry Suite (ACS) composed of spectroscopic instruments for the inspection of the Martian surface in the infrared spectral range (Korablev et al., 2018). ACS is a set of three spectrometers (NIR, MIR and TIRVIM) that are observing Mars in three modes: solar occultation, nadir and limb geometry. The ACS TIRVIM channel is a 2-inch double pendulum thermal infrared Fourier-transform spectrometer, like his ancestors TES and PFS, with cryogenically cooled detector covering the spectral range between 1.7 and 17 μm with apodized resolution that varies from 0.2 to 1.3 cm^{-1} (Korablev et al., 2018). TIRVIM has capabilities that are for several aspects similar to those of IRIS (Mariner 9), TES and PFS instruments but it has advantages related to: - a highest spectral resolution; - a better noise equivalent radiance (from 0.08 $\text{mW}/\text{m}^2/\text{sr}^{-1}/\text{cm}^{-1}$); - a dense spatial coverage (Korablev et al., 2018). TGO has in fact a 400 km altitude quasi-circular orbit with an inclination of 74° and performs 12 orbits per day, having an orbital period of ~2 hr. In a day and at a given latitude, TGO samples 24 different longitudes. TIRVIM nadir tracks provide sampling of the entire planet except for the polar regions (Guerlet et al., 2022). The TIRVIM instrument has an altitude sensitivity that goes from the surface to 60 km (with a vertical resolution of 3 km near the surface to 20 km at high latitudes) (Ignatiev et al., 2018). Temperature profiles from the Martian surface up to 50–60 km,

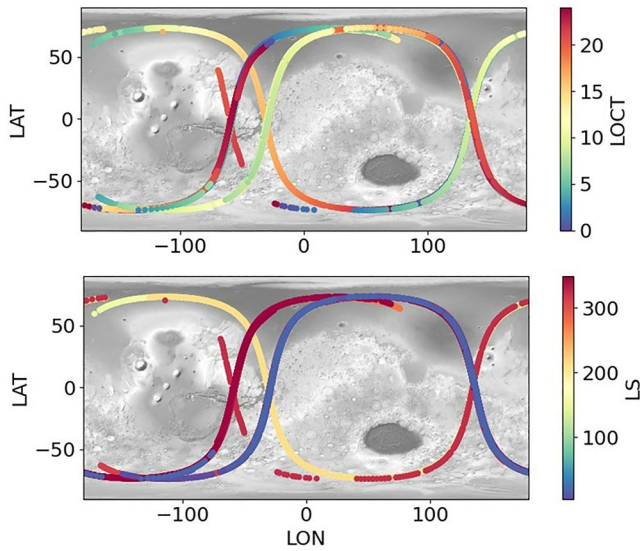


Figure 1. Geographic distribution of the dataset analyzed in this work in terms of latitude (y -axis), longitude (x -axis) and local time (z -axis) in the upper panel, and Solar longitude (LS, z -axis) in the lower panel. Footprints are shown with color ranging from blue to red and linked to the LOCT and LS values, respectively (scale on the right). The background map is a gray-scale MOLA topographic mosaic. An equidistant cylindrical map projection is used at low latitudes, while a sinusoidal and polar stereographic projection is applied at mid to high latitudes.

along with dust and water ice optical depths, can be retrieved through the observation of the CO_2 15- μm band in TIRVIM nadir observation mode. In addition, surface temperature can be retrieved from the data. In solar occultation mode, TIRVIM allows distinguishing between mineral and condensate aerosols (CO_2 — H_2O —dust particles) in the Martian atmosphere, providing profiles of CO_2 , CO , H_2O and aerosols (Korablev et al., 2018). TIRVIM performs in-flight calibrations alternating observations of deep space and the use of an internal calibration body (Ignatiev et al., 2018).

3. Methodology

To analyze the ExoMars TIRVIM data and to recover and identify the number of the various atmospheric contributions present in these data and their spectral shape (by means of spectral indicators, e.g., wavelength positions, band depths, half width; slopes), a methodology has been applied based on a combination of PCA and TT techniques (D'Amore et al., 2013; Bandfield et al., 2000). It has been shown that through the application of these techniques it is possible to extract the composition of laboratory samples (Smith et al., 1985); to extract the main varying components from a big thermal infrared spectral data set (Bandfield et al., 2000), and then to identify them as components of the atmosphere and separate their contribution from surface emission (Smith et al., 2000). This methodology, previously successfully used for the analysis of TES and PFS data (D'Amore et al., 2013; Maturilli et al., 2009), has been, here, applied to the analysis of the new and at higher spectral resolution TIRVIM data set.

To analyze the TIRVIM data and retrieve the atmospheric components, the following steps have been performed:

- Selection of the data set to be analyzed - As starting point for the analysis performed in this work, we selected TIRVIM data acquired along the orbits that cross Elysium Planitia, landing site of the NASA's Insight (Interior exploration using Seismic Investigations, Geodesy and Heat Transport) lander, for possible future comparison with these data. The selected data orbits cover almost a Martian Year (MY) between mid-MY 34 and the beginning of MY 35. For MY34, Ls spans from 150° to 350° , covering part of the Martian northern hemisphere summer and of the Martian autumn and winter, going through the autumn equinox and the winter solstice in the northern hemisphere of the planet. For MY34, Ls span from 4° to 20° covering part of the Martian Northern hemisphere spring. Corresponding Local Times (LOCT) go from Martian day to Martian night (see Figure 1).

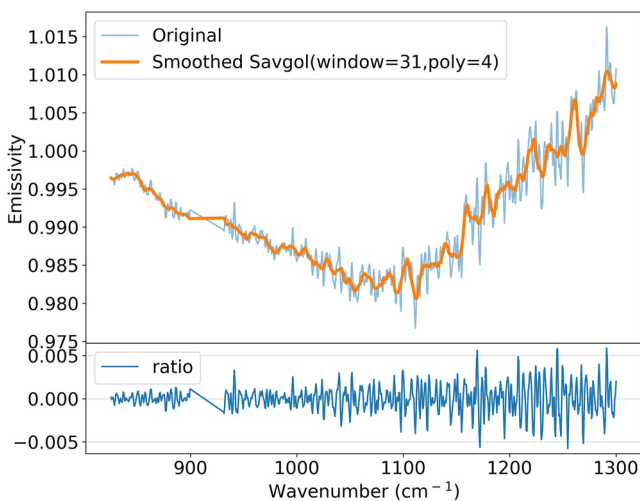


Figure 2. Upper panel: comparison between a TIRVIM retrieved emissivity spectrum (blue line) and a smoothed spectrum obtained by applying a Savitzky–Golay filter (Savitzky and Golay, 1964 and Virtanen et al., 2020) with a window length of 31 and a polyorder (i.e., the order of the polynomial used to fit the spectra) of 4. Bottom panel: ratio between the original and the smoothed spectrum.

- Emissivity retrieval and cleaning/smoothing of the data - the data selected have been cleaned from instrumental spikes present around ~ 900 – 930 cm^{-1} ; ~ 1600 – 1632 cm^{-1} and ~ 1977 – 1984 cm^{-1} . A smoothing function, based on a Savitzky–Golay filter (Savitzky and Golay., 1964; Virtanen et al., 2020) has been applied to the data to reduce general instrumental noise. Smoothed spectra compared with original spectra between ~ 830 and 1300 cm^{-1} , are shown in Figure 2. Emissivity has been obtained by dividing the observed spectra by a Planck curve derived with the highest brightness temperature found around 1255 cm^{-1} for all the spectra. The T surface has been obtained as the median of T brightness in the range 1245 – 1255 cm^{-1} .
- Identification of the principal varying components - this represents a critical task and various methods have been tested to identify the correct number of principal components. In this work, a combination of three methods has been used: (a) eigenvalues ratio (Bandfield et al., 2000);

Table 1
List of Eigenvalues, Variance, Explained Variance (Variance Ratio), Cumulative Sum of Explained Variance (Cumulative Variance Ratio) and Variance Ratio Difference (Variance Ratio Diff) Obtained for the First Eight Extracted Eigenvectors

	Eigenvalue	Variance	Variance ratio	Cumulative variance ratio	Variance ratio Diff
0	135.788849	1.233682	0.768473	0.768473	NaN
1	30.811214	0.063517	0.039566	0.808039	-0.728908
2	29.560771	0.058466	0.036419	0.844458	-0.003146
3	14.530939	0.014127	0.008800	0.853259	-0.027619
4	12.841887	0.011034	0.006873	0.860132	-0.001927
5	11.397865	0.008692	0.005414	0.865546	-0.001459
6	11.137494	0.008299	0.005170	0.870716	-0.000245
7	10.723799	0.007694	0.004793	0.875509	-0.000377

(b) reconstruction error (Malinkosky, 2002); (c) visual inspection of the spectra. The use of these techniques allows to extract eigenvectors and eigenvalues from the covariance matrix and to write the measurements in the form: $D = R \cdot C$, D is the data matrix, R is the matrix of reconstructing vectors and C is the concentration coefficient matrix.

- Identification of the spectral end-members - once eigenvectors and eigenvalues are retrieved, a physical meaning should be assigned to each principal component vector obtained, by assigning it to a spectrum of an actual specimen (D'Amore et al., 2013). In this step, a Target Transformation (TT) has been applied that consists in a translation of the R matrix by rotation in a set of physically significant vectors. The R matrix projects x_n on a set of test vectors: $x_b = R \cdot t_n$, where t_n is the spectrum from a trial library and x_n is the trial spectrum projected in the space generated by R (D'Amore et al., 2013; Bandfield et al., 2000).
- Comparison with results obtained from TES data - the spectral end-members identified applying this methodology to TIRVIM data have been compared with those obtained from previous analysis of TES data.

4. Application to TIRVIM Data and Results

The methodology described in the previous section, has been applied to a subset of TIRVIM data (as discussed in Section 2), with the main goal of verifying that TIRVIM data can be successfully described through linear combination of the recovered TIRVIM atmospheric end-members.

Considering that the PCA works at its best when the different components show significant variation in the data, we made sure that our subset of selected TIRVIM data cover orbits where such variations could more likely occur. In fact, as already mentioned in Section 2, the selected dataset covers a diurnal as well as seasonal variation, spanning from day to night and from part of the Martian summer to part of the Martian autumn (see Figure 1).

Following the application of the PCA (Pedegrosa et al., 2011), it has been possible to successfully extract the independent eigenvectors of the dataset. We analyzed 14,920 Martian TIRVIM spectra. Each TIRVIM spectrum was compressed from 695 components or wavelengths to 45 principal components coefficients, while retaining 96% of the original data variance. Eigenvalues decrease rapidly in the first components but after PCA.7, the ratio starts to decrease slowly. For this reason, we decided to consider the eigenvectors from PCA.8 as secondary respect to the ones before, because they do not show any signature and instead only detect noise present in the data while the first 8 eigenvectors capture the main variations present in the data set. For each of these 8 components, values of eigenvalues, variance, explained variance (percentage of variance) and cumulative sum of explained variance are listed in Table 1. The spectra of these eigenvectors are shown in Figure 3.

These eight eigenvectors capture variations in the data associated with the presence of water ice and dust in the Martian atmosphere. After applying the PCA, a list of general TES atmospheric end-members extracted in Bandfield et al. (2000) and D'Amore et al. (2013) have been used as initial guess for the TT, to interpret the abstract eigenvectors retrieved from the PCA and give them a physically coherent meaning.

The following TES retrieved atmospheric end members have been used:

- DUST_HIGH_CO2_TES: atmospheric dust emissivity with high pressure (Bandfield et al., 2000; D'Amore et al., 2013) (on Mars mainly CO_2).
- DUST_LOW_CO2_TES: atmospheric dust emissivity with low pressure (D'Amore et al., 2013) (on Mars mainly CO_2).

The Martian atmosphere is composed for the ~95% of CO_2 (Mahaffy et al., 2013; Owen et al., 1997) and it has been showed that ~25%–30% of the atmosphere is cycled every year through the seasonal cups (Forget & Pollack, 1996; Kelly et al., 2006; Prettyman et al., 2009; Tillman et al., 1993; Titus et al., 2017). The CO_2 cycle has a strong influence on the Martian atmosphere and climate together with the H_2O cycle and the dust cycle (Titus et al., 2017). These last two cycles interact and modify the CO_2 cycle: - dust can change the albedo and emissivity of CO_2 , ice and snow; - subsurface H_2O ice can act as thermal capacitor reducing the

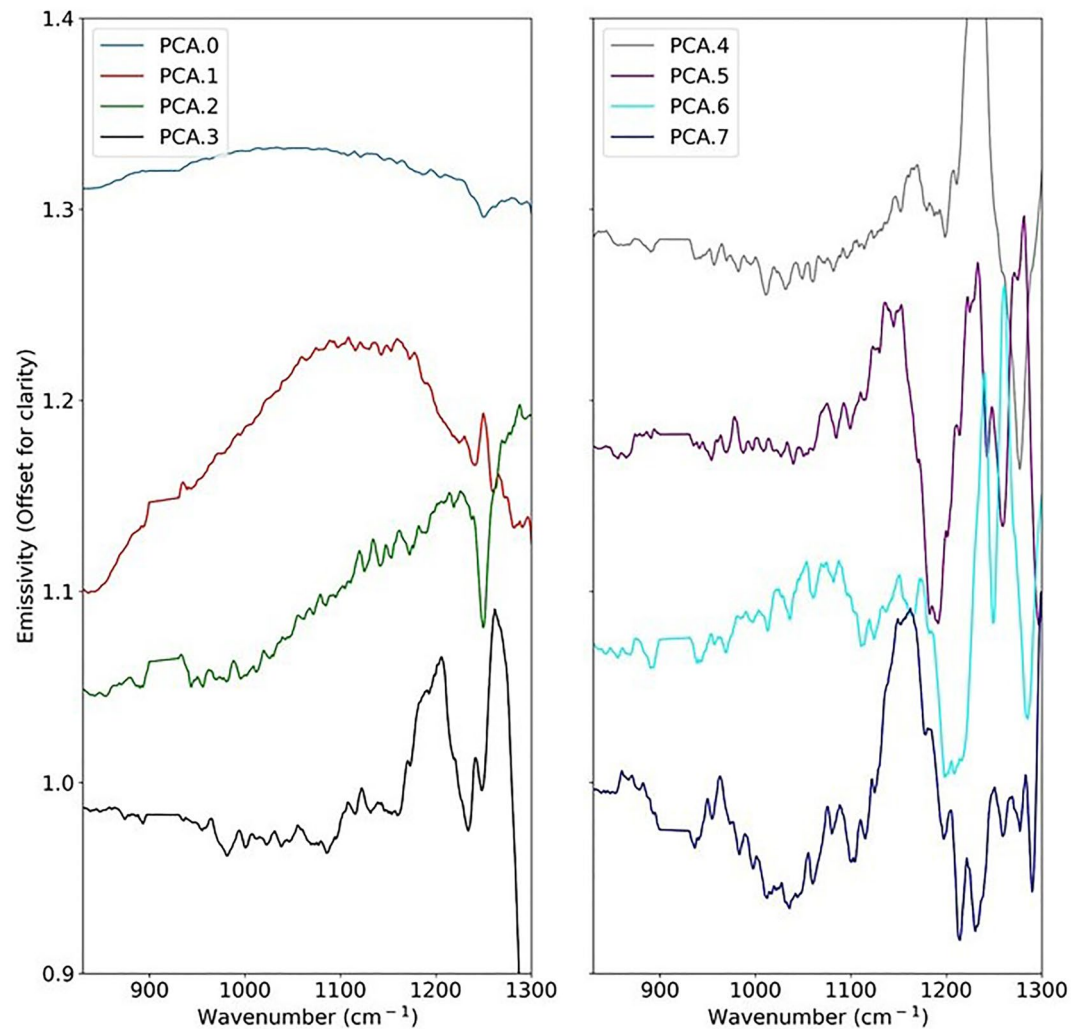


Figure 3. Extracted eigenvectors from the studied TIRVIM data. Left panel: from the top, the first eigenvector (PCA.0—blue) and subsequent principal eigenvectors (PCA.1—red; PCA.2—green; PCA.3). Right panel: from the fifth extracted eigenvector to the subsequent ones (PCA. 4—gray; PCA.5—purple; PCA.6—cyan; PCA.7—dark blue). Offset on the Y-axis has been added for clarity (the spectra lines are shifted from each other by a factor of 0.1).

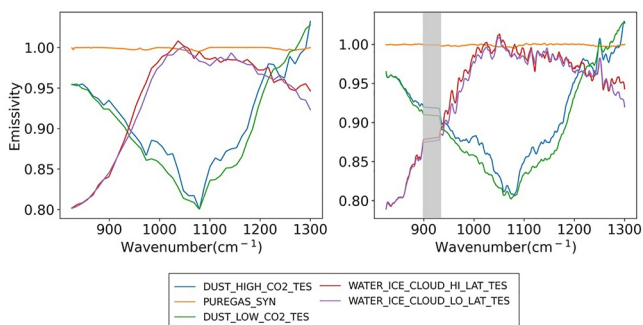


Figure 4. Comparison between the general TES extracted endmembers (Bandfield et al., 2000; D’Amore et al., 2013) (left panel) and the endmembers extracted from the TIRVIM data in this work (right panel). Gray area: wavenumber cut due to high instrumental noise.

accumulation of CO₂ in winter and fall (Haberle et al., 2008). Moreover, it has been observed that the mass distribution of CO₂ gas and solid ice phases shows variations not only seasonally but also over longer timescales as results of orbital changes such as changes in obliquity and changes in other orbital parameters that affect the planet insolation and in turn the CO₂ cycle itself (Tillman et al., 1993).

- WATER_ICE_CLOUD_HI_LAT_TES: atmospheric water ice emissivity at high latitudes (D’Amore et al., 2013).
- WATER_ICE_CLOUD_LO_LAT_TES: atmospheric water ice emissivity at low (equatorial) latitudes (D’Amore et al., 2013).
- PUREGAS_SYN: pure Mars atmospheric gases (mainly CO₂, H₂O) synthetic transmittance spectrum, calculated using a correlated-k method (Ignatiev et al., 2005).

The results obtained from the TT applied on TIRVIM data are shown in Figure 4 (right panel) in comparison with the TES endmembers (Figure 4, left panel and Figure 5).

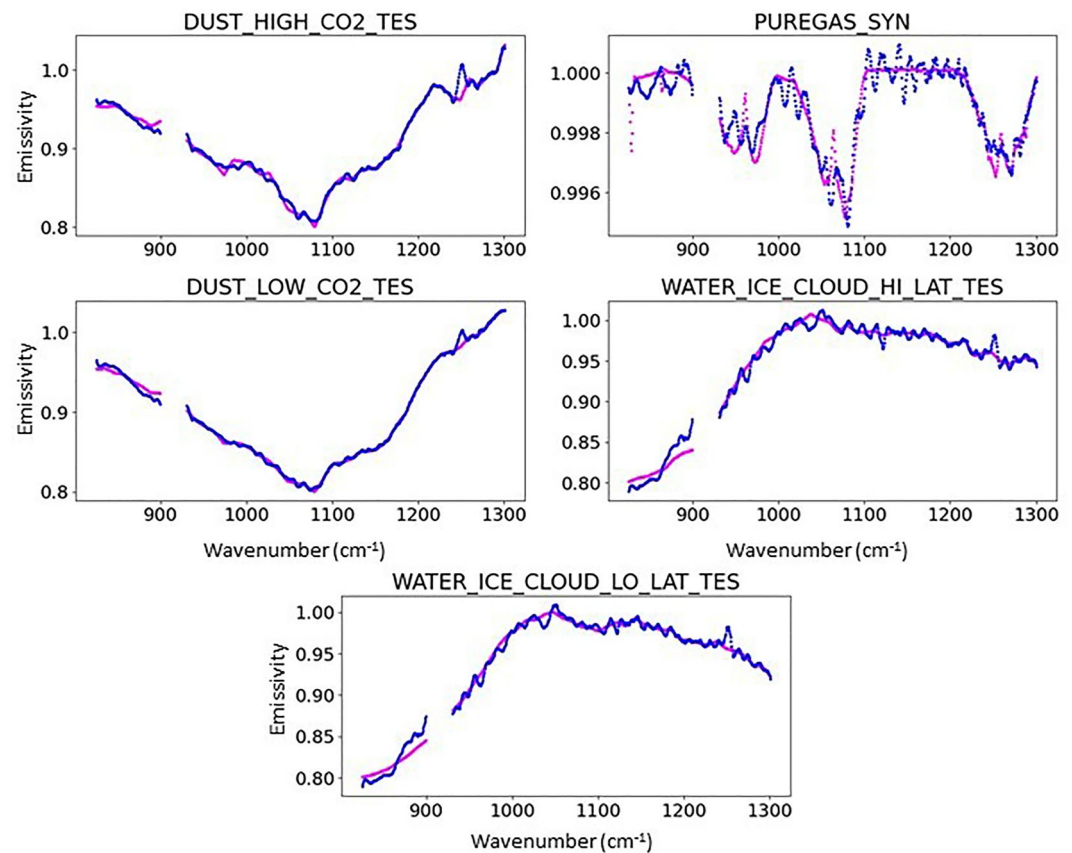


Figure 5. Comparison between the TES extracted endmembers (magenta) (D'Amore et al., 2013) and the endmembers extracted from the TIRVIM data (blue) (this work).

Results obtained from the TT show that the dust and water-ice spectral shapes closely match and describe their projection into the TIRVIM eigenvectors space (Figure 5): this is especially true for the endmembers DUST_LOW_CO2_TES and DUST_HIGH_CO2_TES. A broad band centered around 1080 cm^{-1} is visible in TIRVIM data as well as in TES data. Small differences in the appearance of this band can be due to a lower dust opacity in the used dataset that produces a dust spectrum with a lower intensity (DUST_LOW_CO2_TES). The presence of water ice is also well constrained: a close match has been detected for the water ice TES endmembers (WATER_ICE_CLOUD_HI_LAT, WATER_ICE_CLOUD_LO_LAT) spectral shapes. The ice endmember has an absorption centered around 800 cm^{-1} : even though the absorption band cannot be entirely visible in the investigated spectral range, it has been possible to detect a clear decrease in intensity that well matches with the one retrieved from TES data. As for the dust, also water ice exhibits spectral shapes slightly different from high and low latitudes. Small differences can also be explained considering that a partial mixing of these two components cannot be entirely excluded and can be mainly due to a subtle spatial correlation between the variation of these two components in the data set selected. Smaller features can also be matched to Martian atmospheric gases as for the ones visible projecting the PUREGAS_SYN endmember into the TIRVIM eigenvectors space. PUREGAS_SYN endmember shows the influence of faint CO_2 bands (note the different scale variation in the top right panel of Figure 5 compared to the other plots in the same figure), visible especially from the doublets centered around 960 and 1070 cm^{-1} , and the doublet near 1250 cm^{-1} .

Overall, there is a good match between the target-transformed TIRVIM spectra and the endmembers used as initial guess (see Figure 5): this indicates that the retrieved TIRVIM end-members closely match the initial TES guess vectors.

Moreover, comparing our results on atmospheric component retrieval on TIRVIM data with the ones previously obtained on TES data (Bandfield et al., 2000), allows us to assess the stability of the dust and water ice components on a large timescale. Retrieved atmospheric components from TES have been compared with PFS

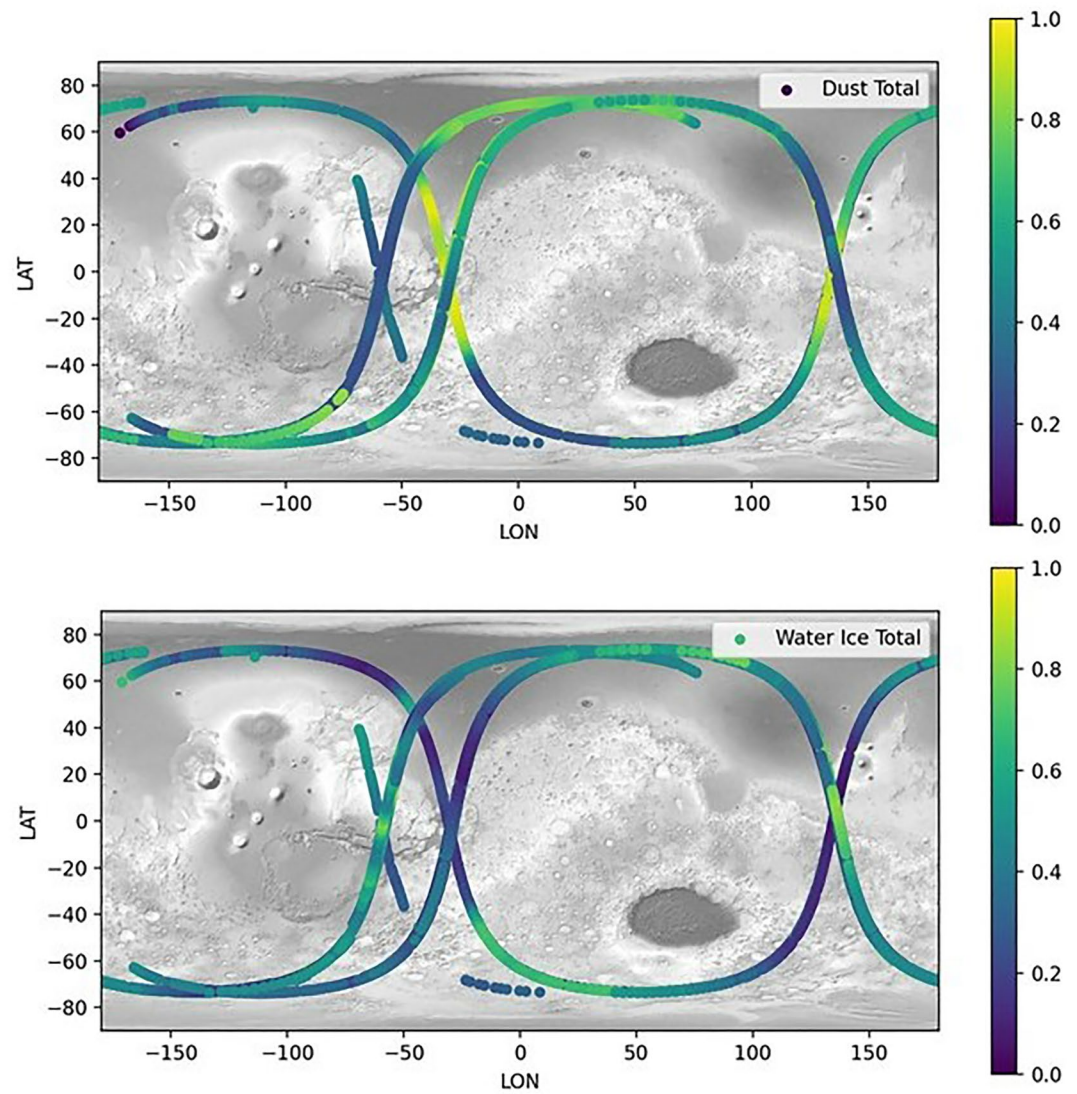


Figure 6. Upper panel: Geographic distribution of the total dust endmember (normalized) in terms of latitude (y-axis), longitude (x-axis). Bottom panel: Same as in the upper panel but for the total water ice endmember (normalized). The background map is a gray scale MOLA topographic mosaic. Map projection same as in Figure 1. Footprints are shown with color ranging from purple for minimum values to yellow for maximum values of concentration (scale on the right).

and IRIS data, hence showing that the extracted eigenvectors do not show significant variation over almost 30 years of observations of the Red Planet (D'Amore et al., 2013). The comparison of our results with the one obtained from IRIS, TES and PFS data allows us to extend the study of the stability of the Martian atmospheric components even on a larger timescale: IRIS data contain information on the atmospheric components during 1971, while TES observed the Martian atmosphere from 1997 to 2006, PFS observations started in 2004 while TIRVIM observed the Martian atmosphere from mid-2018 to almost the end of 2019. We can therefore assess the stability of the retrieved components in the Martian atmosphere over a period of almost 50 years.

4.1. Retrieval of Concentration Coefficients and Abundance Maps

The original spectra were deconvolved through linear unmixing of the recovered spectral end-members to obtain the concentration coefficients of the dust and water ice end-members. The deconvolution adopted consists of a Fully Constrained Least Squares fit (FCLS) (Heinz & Chang, 2001; Heinz et al., 1999; Therien, 2018).

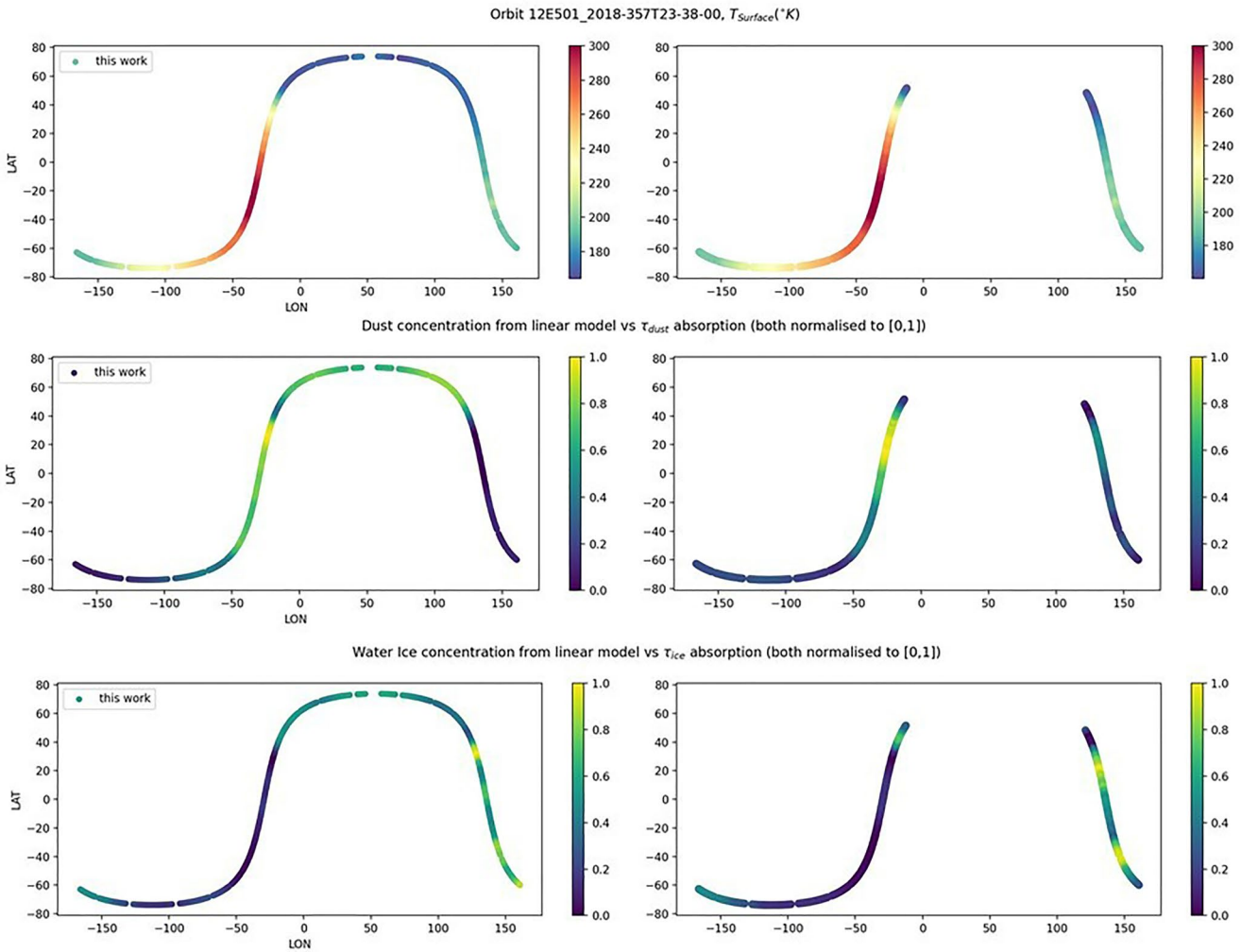


Figure 7. Comparison of our results (on the left) with values retrieved in Guerlet et al. (2022) from processed TIRVIM data (on the right) and available on the Institut Pierre Simon Laplace data server (see in Guerlet et al., 2022). From top to bottom comparison of: - T_{surface} values from our work versus T_{surface} values from Guerlet et al. (2022); - dust concentration from linear model versus τ_{dust} from Guerlet et al. (2022) (both normalized to [0,1]); - water ice concentration from linear model versus $\tau_{\text{water ice}}$ from Guerlet et al. (2022) (both normalized to [0,1]).

In order to obtain accurate amounts of abundances, FCSL imposes two constraints on the abundances retrieved by the model: the abundance sum-to-one constraint (ASC) and the abundance non-negativity constraint (ANC) for each spectrum.

Retrieved abundance distributions of the endmembers DUST_LOW_CO2 and WATER_ICE_CLOUD_HIGH in our data with LAT and LON, are shown in Figure 6.

T_{surface} values and concentration coefficients retrieved in this work have been compared with T_{surface} and optical depths retrieved for dust and water ice (τ_{dust} and $\tau_{\text{water ice}}$) from Guerlet et al. (2022) on the same orbits (see Figure 7). These authors applied a radiative transfer retrieval algorithm to TIRVIM nadir viewing geometry spectra, to estimate Martian surface temperatures and obtain vertical profiles of the Martian atmospheric temperature and optical depths of dust and water ice clouds. The comparison (Figure 7) shows a good consistency between the surface temperature values and dust/water ice concentration obtained with the two different methods (high $\tau =$ high concentrations). Most of the differences found between retrieved dust and water ice abundances could be attributed to the lower signal in the spectra due to the lower surface temperature.

Moreover, the results obtained in this work show that through linear combination of the retrieved endmembers it is possible to obtain with high accuracy a reconstruction of the spectral features present in the TIRVIM original

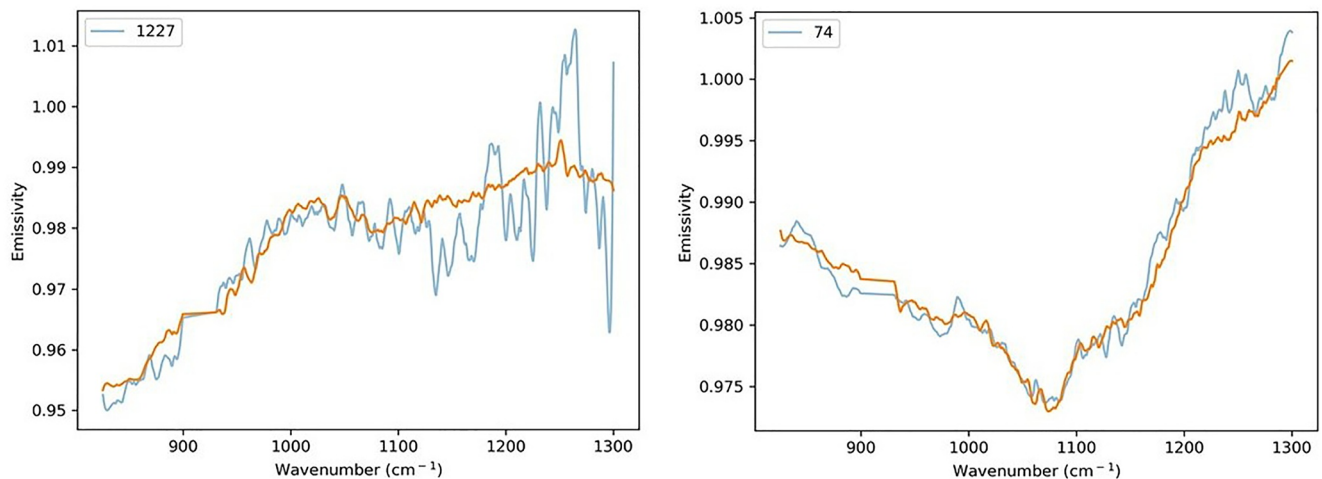


Figure 8. Examples of comparison between original TI Thermal Infrared channel spectra (in blu) and the reconstructed ones through linear combination of the retrieved endmembers (in orange).

data. Same examples of reconstructed spectra compared with original spectra are shown in Figure 8. Retrieved concentration coefficients of the endmembers used to reconstruct the spectra in Figure 8 are reported in Table 2.

5. Conclusion and Future Developments

In this paper, a first successful application of PCA and TT techniques to high-resolution TIRVIM data is presented, showing how these data can be successfully modeled through a linear combination of a limited set of recovered atmospheric end-members. The results obtained in this work show, in fact, that the methodology applied can successfully identify the number of independently variable components present in the TIRVIM data and recover the associated spectral end-members: spectral shapes of both atmospheric dust and water ice aerosols can be recognized. Moreover, the comparison between our results on TIRVIM data, with those previously obtained on PFS and IRIS data (D’Amore et al., 2013) and those obtained on TES data (Bandfield et al., 2000) allowed us to assess the temporal stability and homogeneity of dust and water ice in the Martian atmosphere over a time period of almost 50 years.

The results obtained here are promising and have a potential outcome in terms of further understanding of the Martian atmosphere as well as potentially of the planet surface: - aerosol properties and abundances in the Martian atmosphere strongly influence the Martian climate; - identification and separation of the atmospheric components, have strong impact on the potential identification of surface contributions in the spectra. We aim at further investigating TIRVIM data in follow-up works with the main goal of showing the potential of this methodology to extract valuable information not only on the atmosphere but also on the surface of the Red Planet in the thermal infrared spectral region. For this purpose, the next planned step involves the application of our laboratory

Table 2

Concentration of Coefficients of the Endmembers: Blackbody, DUST_HIGH_CO2, DUST_LOW_CO2, PUREGAS_SYN, WATER_ICE_CLOUD_HL (High Latitudes), WATER_ICE_CLOUD_LL (Low Latitudes) Along With Rec_Diff_Per_Spectra (= rms Data to Linear Model) and Rms_to_Ext_Smooth (=rms Data Smoothed to Data Smoothed), for the Spectra in Figure 8

Spectrum	Blackbody	DUST_HIGH_CO2	DUST_LOW_CO2	PUREGAS_SYN
74	3.511	0.098	0.504	0.238
1227	2.239	0.001	0.318	0.001
	WATER_ICE_CLOUD_HL	WATER_ICE_CLOUD_LL	rec_diff_per_spectra	rms_to_ext_smooth
74	0.097	0.063	0.006	0.003
1227	0.011	0.669	0.020	0.013

spectral library (Alemanno et al., 2021) of Mars analogs as a trial library for the TT to recover the different surface components from TIRVIM data. The results and analysis performed in this work are also thought in the framework of the interpretation of spectral data coming from future missions from Mars.

Data Availability Statement

The processed TIRVIM data and retrievals used in this paper are available on the zenodo server. See: <https://doi.org/10.5281/zenodo.7032738>.

Acknowledgments

The ACS experiment, part of ExoMars space mission (ESA and Roscosmos), is led by IKI (Space Research Institute, Moscow) assisted by LATMOS (France). Science operations of ACS are funded by Roscosmos and ESA. The authors acknowledge Sandrine Guerlet and the ACS/TGO team for supplying the data for the comparison and the data center ESPRI/IPSL for their help in accessing the data. Open Access funding enabled and organized by Projekt DEAL.

References

- Adler, H. H., & Kerr, P. F. (1962). Infrared study of aragonite and calcite. *American Mineralogist*, *47*, 700–717.
- Alemanno, G., Maturilli, A., D'Amore, M., & Helbert, J. (2021). A new laboratory emissivity and reflectance spectral library for the interpretation of Mars thermal infrared spectral data. *Icarus*, *368*, 114622. <https://doi.org/10.1016/j.icarus.2021.114622>
- Bandfield, J. L. (2002). Global mineral distributions on Mars. *Journal of Geophysical Research*, *107*(E6), 5042. <https://doi.org/10.1029/2001JE001510>
- Bandfield, J. L., Christensen, P. R., & Smith, M. D. (2000). Spectral data set factor analysis and end-member recovery: Application to analysis of Martian atmospheric particulates. *Journal of Geophysical Research*, *105*(E4), 9573–9587. <https://doi.org/10.1029/1999je001094>
- Bandfield, J. L., & Smith, M. D. (2003). Multiple emission angle surface-atmosphere separations of Thermal Emission Spectrometer data. *Icarus*, *161*(1), 47–65. [https://doi.org/10.1016/s0019-1035\(02\)00025-8](https://doi.org/10.1016/s0019-1035(02)00025-8)
- Bibring, J. P., Langevin, Y., Mustard, J. F., Poulet, F., Arvidson, R., Gendrin, A., et al. (2006). Global mineralogical and aqueous Mars history derived from OMEGA/Mars express data. *Science*, *312*(5772), 400–404. <https://doi.org/10.1126/science.1122659>
- Christensen, P. R. (1998). Variations in Martian surface composition and cloud occurrence determined from thermal infrared spectroscopy: Analysis of Viking and Mariner 9 data. *Journal of Geophysical Research*, *103*(E1), 1733–1746. <https://doi.org/10.1029/97je02114>
- Christensen, P. R., Anderson, D. L., Chase, S. C., Clancy, R. T., Clark, R. N., Conrath, B. J., et al. (1998). Results from the Mars global surveyor thermal emission spectrometer. *Science*, *279*(5357), 1692–1698. <https://doi.org/10.1126/science.279.5357.1692>
- Christensen, P. R., Anderson, D. L., Chase, S. C., Clark, R. N., Kieffer, H. H., Malin, M. C., et al. (1992). Thermal emission spectrometer experiment: Mars observer mission. *Journal of Geophysical Research*, *97*(E5), 7719–7734. <https://doi.org/10.1029/92je00453>
- Christensen, P. R., Mehall, G. L., Silverman, S. H., Anwar, S., Cannon, G., Gorelick, N., et al. (2003). Miniature thermal emission spectrometer for the Mars exploration Rovers. *Journal of Geophysical Research*, *108*(E12), 8064. <https://doi.org/10.1029/2003JE002117>
- Conrath, B., Curran, R., Hanel, R., Kunde, V., Maguire, W., Pearl, J., et al. (1973). Atmospheric and surface properties of Mars obtained by infrared spectroscopy on Mariner 9. *Journal of Geophysical Research*, *78*(20), 4267–4278. <https://doi.org/10.1029/jb078i020p04267>
- D'Amore, M., Maturilli, A., Zinzi, A., Palomba, E., & Helbert, J. (2013). Martian atmospheric particulate spectral end-members recovery from PFS and IRIS data. *Icarus*, *226*(2), 1294–1303. <https://doi.org/10.1016/j.icarus.2013.08.002>
- Feely, K. C., & Christensen, P. R. (1999). Quantitative compositional analysis using thermal emission spectroscopy: Application to igneous and metamorphic rocks. *Journal of Geophysical Research*, *104*(E10), 24195–24210. <https://doi.org/10.1029/1999je001034>
- Forget, F., & Pollack, J. B. (1996). Thermal infrared observations of the condensing Martian polar caps: CO₂ ice temperatures and radiative budget. *Journal of Geophysical Research*, *101*(E7), 16865–16880. <https://doi.org/10.1029/96je01077>
- Formisano, V., Angrilli, F., Arnold, G., Atreya, S., Bianchini, G., Biondi, D., et al. (2005). The planetary fourier spectrometer (PFS) onboard the European Mars express mission. *Planetary and Space Science*, *53*(10), 963–974. <https://doi.org/10.1016/j.pss.2004.12.006>
- Gillespie, A. R. (1992). Spectral mixture analysis of multispectral thermal infrared images. *Remote Sensing of Environment*, *42*(2), 137–145. [https://doi.org/10.1016/0034-4257\(92\)90097-4](https://doi.org/10.1016/0034-4257(92)90097-4)
- Guerlet, S., Ignatiev, N., Forget, F., Fouchet, T., Vlasov, P., Bergeron, G., et al. (2022). Thermal structure and aerosols in Mars' atmosphere from TIRVIM/ACS onboard the ExoMars Trace Gas Orbiter: Validation of the retrieval algorithm. *Journal of Geophysical Research: Planets*, *127*(2), e2021JE007062. <https://doi.org/10.14768/ab765eba-0c1d-47b6-97d6-6390c63f0197>
- Haberle, R. M., Forget, F., Colaprete, A., Schaeffer, J., Boynton, W. V., Kelly, N. J., & Chamberlain, M. A. (2008). The effect of ground ice on the Martian seasonal CO₂ cycle. *Planetary and Space Science*, *56*(2), 251–255. <https://doi.org/10.1016/j.pss.2007.08.006>
- Hamilton, V. E., & Christensen, P. R. (2000). Determining the modal mineralogy of mafic and ultramafic igneous rocks using thermal emission spectroscopy. *Journal of Geophysical Research*, *105*(E4), 9717–9734. <https://doi.org/10.1029/1999je001113>
- Hamilton, V. E., Christensen, P. R., & McSween, H. Y., Jr. (1997). Determination of Martian meteorite lithologies and mineralogies using vibrational spectroscopy. *Journal of Geophysical Research*, *102*(E11), 25593–25603. <https://doi.org/10.1029/97je01874>
- Hanel, R., Conrath, B., Hovis, W., Kunde, V., Lowman, P., Maguire, W., et al. (1972). Investigation of the Martian environment by infrared spectroscopy on Mariner 9. *Icarus*, *17*(2), 423–442. [https://doi.org/10.1016/0019-1035\(72\)90009-7](https://doi.org/10.1016/0019-1035(72)90009-7)
- Heinz, D. C., & Chang, C. (2001). Fully constrained least squares linear spectral mixture analysis method for material quantification in hyperspectral imagery. *IEEE Transactions on Geoscience and Remote Sensing*, *39*(3), 529–545. <https://doi.org/10.1109/36.911111>
- Heinz, D. C., Chang, C., & Mark, L. G. (1999). Fully constrained least-squares based linear unmixing. *Athhouse*. IEEE.
- Huang, C. K., & Kerr, P. F. (1960). Infrared study of the carbonate minerals. *American Mineralogist*, *45*, 311–324.
- Ignatiev, N., Grigoriev, A., & Shakun, A. (2018). *Monitoring of the atmosphere of Mars with ACS TIRVIM nadir observations on ExoMars TGO* (pp. EPSC2018–891). European Planetary Science Congress.
- Ignatiev, N. I., Grassi, D., & Zasova, L. V. (2005). Planetary Fourier Spectrometer data analysis: Fast radiative transfer models. *Planetary and Space Science*, *53*(10), 1035–1042. <https://doi.org/10.1016/j.pss.2004.12.009>
- Kelly, N., Boynton, W., Kerry, K., Hamara, D., Janes, D., Reedy, R. C., et al. (2006). Seasonal polar carbon dioxide frost on Mars: CO₂ mass and columnar thickness distribution. *Journal of Geophysical Research*, *111*(E3), E03S07. <https://doi.org/10.1029/2006je002678>
- Korablev, O., Montmessin, F., Trokhimovskiy, A., Fedorova, A. A., Shakun, A. V., Grigoriev, A. V., et al. (2018). The atmospheric chemistry suite (ACS) of three spectrometers for the ExoMars 2016 Trace gas orbiter. *Space Science Reviews*, *214*, 7.(
- Luginin, M., Fedorova, A., Ignatiev, N., Trokhimovskiy, A., Shakun, A., Grigoriev, A., et al. (2020). Properties of water ice and dust particles in the atmosphere of Mars during the 2018 global dust storm as inferred from the atmospheric chemistry suite. *Journal of Geophysical Research: Planets*, *125*(11), e2020JE006419. <https://doi.org/10.1029/2020JE006419>

- Mahaffy, P. R., Webster, C. R., & Atreya, S. K. (2013). Abundance and isotopic composition of gases in the Martian atmosphere from the curiosity rover. *Science*, *341*(6143), 263–266.
- Malinkosky, E. R. (2002). Factor Analysis in Chemistry (3rd edn).
- Martin, T. Z., & Richardson, M. I. (1993). New dust opacity mapping from Viking IR Thermal Mapper data. *Journal of Geophysical Research*, *98*(E6), 10941–10949. <https://doi.org/10.1029/93je01044>
- Maturilli, A., Helbert, J., & D'Amore, M. (2009). *Phyllosilicates detection in Syrtis Major and Mawrth Vallis of Mars from PFS measured spectra*. EPSC Conference.
- Maturilli, A., Helbert, J., & Moroz, L. (2008). The Berlin emissivity database (BED). *Planetary and Space Science*, *56*(3–4), 420–425. <https://doi.org/10.1016/j.pss.2007.11.015>
- Murchie, S. L., Arvidson, R., Bedini, P., Beisser, K., Bibring, J. P., Bishop, J., et al. (2007). Compact reconnaissance imaging spectrometer for Mars (CRISM) on Mars reconnaissance orbiter (MRO). *Journal of Geophysical Research*, *112*(E5), E05S03. <https://doi.org/10.1029/2006JE002682>
- Owen, T., Biemann, K., Rushneck, D., Biller, J. E., Howarth, D. W., & Lafleur, A. L. (1997). The composition of the atmosphere at the surface of Mars. *Journal of Geophysical Research*, *82*(28), 4635–4639. <https://doi.org/10.1029/jg082i028p04635>
- Pedregosa, F., Varoquaux, G., Gramfort, A., Michel, V., Thirion, B., Grisel, O., et al. (2011). Scikit-learn: Machine learning in Python. *Journal of Machine Learning Research*, *12*, 2825–2830.
- Poulet, F., Bibring, J. P., Mustard, J. F., Gendrin, A., Mangold, N., Langevin, Y., et al. (2005). Phyllosilicates on Mars and implications for early Martian climate. *Nature*, *438*(7068), 623–627. <https://doi.org/10.1038/nature04274>
- Prettyman, T. H., Feldman, W. C., & Titus, T. N. (2009). Characterization of Mars' seasonal caps using neutron spectroscopy. *Journal of Geophysical Research*, *114*(E8), E08005. <https://doi.org/10.1029/2008je003275>
- Ramsey, M. S., & Christensen, P. R. (1998). Mineral abundance determination: Quantitative deconvolution of thermal emission spectra. *Journal of Geophysical Research*, *103*(B1), 577–596. <https://doi.org/10.1029/97jb02784>
- Ramsey, M. S., Christensen, P. R., Lancaster, N., & Howard, D. A. (1999). Identification of sand sources and transport pathways at Kelso Dunes, California using thermal infrared remote sensing. *The Geological Society of America Bulletin*, *111*(5), 636–662. [https://doi.org/10.1130/0016-7606\(1999\)111<0646:iosat>2.3.co;2](https://doi.org/10.1130/0016-7606(1999)111<0646:iosat>2.3.co;2)
- Ramsey, M. S., & Fink, J. H. (1999). Estimating silicic lava vesicularity with thermal remote sensing: A new technique for volcanic mapping and monitoring. *Bulletin of Volcanology*, *61*(1–2), 32–39. <https://doi.org/10.1007/s004450050260>
- Savitzky, A., & Golay, M. J. E. (1964). Smoothing and differentiation of data by simplified least squares procedures. *Analytical Chemistry*, *36*(8), 1627–1639. <https://doi.org/10.1021/ac60214a047>
- Smith, M. D., Bandfield, J. L., & Christensen, P. R. (2000). Separation of atmospheric and surface spectral features in Mars global surveyor thermal emission spectrometer (TES) spectra. *Journal of Geophysical Research*, *85*(E4), 9589–9607. <https://doi.org/10.1029/1999je001105>
- Smith, M. D., Pearl, J. C., Conrath, B. J., & Christensen, P. R. (2000). Mars Global Surveyor Thermal Emission Spectrometer (TES) observations of dust opacity during aerobraking and science phasing. *Journal of Geophysical Research*, *85*(E4), 9539–9552. <https://doi.org/10.1029/1999je001097>
- Smith, M. O., Adams, J. B., & Johnson, P. E. (1985). Quantitative determination of mineral types and abundances from reflectance spectra using principal components analysis. *Journal of Geophysical Research*, *90*(S02), 797–804. <https://doi.org/10.1029/jb090is02p0c797>
- Therien, C. (2018). PySptools. Retrieved from https://pysptools.sourceforge.io/abundance_maps.html
- Thomson, J. L., & Salisbury, J. W. (1993). The mid-infrared reflectance of mineral mixtures (7–14 μm). *Remote Sensing of Environment*, *31*, 1–26. [https://doi.org/10.1016/0034-4257\(93\)90077-b](https://doi.org/10.1016/0034-4257(93)90077-b)
- Tillman, J. E., Johnson, N. C., Guttorp, P., & Percival, D. B. (1993). The Martian annual atmospheric pressure cycle—Years without great dust storms. *Journal of Geophysical Research*, *98*(E6), 10963–10971. <https://doi.org/10.1029/93JE01084>
- Titus, T., Byrne, S., Colaprete, A., Forget, F., Michaels, T., & Prettyman, T. (2017). The CO₂ cycle. In R. Haberle, R. Clancy, F. Forget, M. Smith, & R. Zurek (Eds.), *The atmosphere and climate of Mars* (pp. 374–404). Cambridge University Press. <https://doi.org/10.1017/9781139060172.012>
- Virtanen, P., Gommers, R., Oliphant, T. E., Haberland, M., Reddy, T., Cournapeau, D., et al. (2020). SciPy 1.0: Fundamental algorithms for scientific computing in Python. *Nature Methods*, *17*(3), 261–272. https://docs.scipy.org/doc/scipy/reference/generated/scipy.signal.savgol_filter.html
- Wray, J. J., Murchie, S. L., Bishop, J. L., Ehlmann, B. L., Milliken, R. E., Wilhelm, M. B., et al. (2016). Orbital evidence for more widespread carbonate-bearing rocks on Mars. *Journal of Geophysical Research: Planets*, *121*(4), 652–677. <https://doi.org/10.1002/2015JE004972>
- Wyatt, M. B., Bandfield, J. L., McSween Jr, H. Y., & Christensen, P. R. (2001). Compositions of low albedo intracrater materials and wind streaks on Mars: Examination of MGS TES data in Western Arabia Terra. In *32nd annual lunar and planetary science Conference*.